

Grad-CAM++: Generalized Gradient-based Visual Explanations for Deep Convolutional Networks

Aditya Chattopadhyay*, Anirban Sarkar*, Member, IEEE, Prantik Howlader, and Vineeth N Balasubramanian, Member, IEEE

Abstract—Over the last decade, Convolutional Neural Network (CNN) models have been highly successful in solving complex vision based problems. However, these deep models are perceived as “black box” methods considering the lack of understanding of their internal functioning. There has been a significant recent interest to develop explainable deep learning models, and this paper is an effort in this direction. Building on a recently proposed method called Grad-CAM, we propose a generalized method called Grad-CAM++ that can provide better visual explanations of CNN model predictions, in terms of better object localization as well as explaining occurrences of multiple object instances in a single image, when compared to state-of-the-art. We provide a mathematical derivation for the proposed method, which uses a weighted combination of the positive partial derivatives of the last convolutional layer feature maps with respect to a specific class score as weights to generate a visual explanation for the corresponding class label. Our extensive experiments and evaluations, both subjective and objective, on standard datasets showed that Grad-CAM++ provides promising human-interpretable visual explanations for a given CNN architecture across multiple tasks including classification, image caption generation and 3D action recognition; as well as in new settings such as knowledge distillation.

Index Terms—Explainable AI, Interpretable ML, Convolutional Neural Networks, Computer Vision

1 INTRODUCTION

In recent years, the dramatic progress of machine learning in the form of deep neural networks has opened up new Artificial Intelligence (AI) capabilities in real-world applications. It is no new fact that deep learning models offer tremendous benefits with impressive results in tasks like object detection, speech recognition, machine translation to name a few. However, the connectionist approach of deep learning is fundamentally different from earlier AI systems where the predominant reasoning methods were logical and symbolic. These early systems could generate a trace of their inference steps, which then became the basis for explanation. On the other hand, the effectiveness of today’s intelligent systems is limited by the inability to explain its decisions and actions to human users. This issue is especially important for risk-sensitive applications such as security, clinical decision support or autonomous navigation.

Recent advancements in AI promise to build autonomous systems that perceive, learn, decide and act on their own. However, machine learning today, especially deep learning models, attempt to approximate the function that transforms a given input into the expected output with no explicit knowledge of the function itself, or of the rationale involved in providing a particular output. This makes troubleshooting difficult in case of erroneous behaviour. Moreover, these algorithms are trained on a limited

amount of data which can often be different from data that is presented after training. To this end, various techniques have been undertaken by researchers over the last few years to overcome the dilemma of blindly using deep learning models. One technique is to rationalize/justify the decision of a model by training another deep model which comes up with explanations as to why the model behaved the way it did. Another emerging perspective to such explainable methods is to probe the black-box models by trying to change the input intelligently and analyzing the model’s response to it.

While there have been some promising early efforts in this area (a detailed survey is presented in Section 2), these are cursory and the field of explainable deep learning has a long way to go, considering the difficulty and variety in the problem scope. Zeiler & Fergus [1] initiated efforts in understanding what a CNN (Convolutional Neural Network) learns; however, their method involves significant computations to generate this understanding. Zhou *et al.* [2] showed that various layers of the CNN (Convolutional Neural Network) behave as unsupervised object detectors by a new technique called CAM (Class Activation Mapping). By using a global average pooling [3] layer, and visualizing the weighted combination of the resulting feature maps at the penultimate (pre-softmax) layer, they were able to obtain heat maps that explain which parts of an input image were looked at by the CNN for assigning a label. However, this technique involves retraining a linear classifier for each class. Similar methods were examined with different pooling layers such as global max pooling in [4] and log-sum-exp pooling in [5].

Selvaraju *et al.* [6] came up with an efficient generaliza-

• *These two authors contributed equally to the work.

• A. Chattopadhyay, A. Sarkar and V. Balasubramanian are with the Department of Computer Science and Engineering, Indian Institute of Technology Hyderabad, Telangana, India.

E-mail IDs: {adityac, cs16resch11006, vineethnb}@iith.ac.in

• P. Howlader is with Cisco Systems, Bangalore, India.

tion of CAM, known as Grad-CAM, which fuses the class-discriminative property of CAM with existing pixel-space gradient visualization techniques such as Guided Back-propagation [7] and Deconvolution [1] to highlight fine-grained details on the image. Therefore, Grad-CAM makes CNN-based models more transparent by visualizing input regions with high resolution details that are important for predictions.

While the visualizations generated by gradient-based methods such as Grad-CAM explain the CNN based model prediction with fine-grained details of the predicted class, these methods have limitations - for example, they lack at localizing multiple occurrences of the same class. Even for single object images, Grad-CAM heatmaps fail to localize the entire region of the object. In this work, we propose Grad-CAM++, a generalized visualization technique for interpreting CNN decisions, which ameliorates the aforementioned flaws of earlier methods (elucidated further in section 3) and provides a more general approach. Our key contributions in this work are summarized as follows:

- We introduce pixel-wise weighting of the gradients of the output with respect to a particular spatial position in the final convolutional feature map of the CNN. This approach provides a measure of importance of each pixel in a particular feature map towards the overall decision of the CNN. Importantly, we derive closed-form solutions for the pixel-wise weights, as well as obtain exact expressions for higher order derivatives for both softmax and exponential output activation functions. Our approach requires a single backward pass on the computational graph, thus making it computationally equivalent to prior gradient-based methods while giving better visualizations.
- While several methods exist to visualize CNN decisions, namely, Deconvolution, Guided Back-propagation, CAM, and Grad-CAM, the assessment of the quality of visualizations is done mainly through human evaluations or some auxiliary metric like localization error with respect to bounding boxes (ground truth). This need not correlate with the actual factors responsible for the network's decision. We propose new metrics in this work to evaluate (objectively) the faithfulness of the proposed explanations to the underlying model, i.e., whether the visualization directly correlates with the decision. Our results with these metrics show superior performance of Grad-CAM++ over state-of-the-art.
- A good explanation should be able to effectively distill its knowledge. This aspect of explainable-AI is largely ignored in recent works. We show that in a constrained teacher-student setting, it is possible to achieve an improvement in the performance of the student by using a specific loss function inspired from the explanation maps generated by Grad-CAM++. We introduce a training methodology towards this objective, and show promising results of students trained using our methodology.
- In accordance with previous efforts in visualizing CNNs, we also conduct human studies to test the quality of our explanations. These studies show that

the visualizations produced by Grad-CAM++ instill a greater faith in the underlying model (for the human user) than the corresponding visualizations produced by Grad-CAM.

- Through both visual examples and objective evaluations, we also show that Grad-CAM++ improves upon Grad-CAM in weakly supervised localization of object classes in a given image
- Lastly, we show the effectiveness of Grad-CAM++ in image captioning and 3D action recognition. To the best of our knowledge, visualization of CNN decisions so far have mostly been limited to 2D image data, and this is the first effort on *visual explanations* of 3D-CNNs in video understanding.

The remainder of this paper is organized as follows. Section 2 discusses recent research efforts towards explainability in deep neural network models. Section 3 presents the proposed Grad-CAM++ methodology including the formal design as well as the derivation of the closed-form expressions. Our experimental studies on studying the proposed method against Grad-CAM, the state-of-the-art for gradient-based visualization methods, is presented in Section 4. As part of this section, we also introduce newer evaluation methods for studying such visual explanation methods. Section 5 then describes how explanations obtained from Grad-CAM++ can be used to better train a student network from an expert teacher. Finally, Section 6 illustrates the explanations that Grad-CAM++ can provide for deep models involved in other tasks such as image captioning and 3D action recognition, and Section 7 investigates an important design choice for our methodology.

2 RELATED WORK

Deep learning models have been highly successful in producing impressive results. However, the real bottleneck in accepting most of these techniques for real-life applications is the *interpretability problem*. Usually, these models are treated as black boxes without knowledge of their internal workings. Recently, several methods have been developed to visualize Convolutional Networks and understand what is learnt by each neuron. The most straight-forward technique is to visualize the layer activations, where they generally show sparse and localized patterns. Visualizing the convolution filters is also useful as they reveal the nature of content extracted by the network in a given layer. Another method is to visualize the images which maximally activate a certain neuron in a trained network. This involves a large dataset of images to be fed forward through the network to understand what that neuron is looking for.

Zeiler & Fergus [1] proposed the deconvolution approach to better understand what the higher layers in a given network have learnt. "Deconvnet" makes data flow from a neuron activation in the higher layers, down to the image. In this process, parts of the image that strongly activate that neuron get highlighted. Later, Springenberg *et al.*[7] extended this work to a new method called *guided backpropagation* which helped understand the impact of each neuron in a deep network w.r.t. the input image. These visualization techniques were compared in [8]. Yosinski *et al.*[9] proposed a method to synthesize the input image that

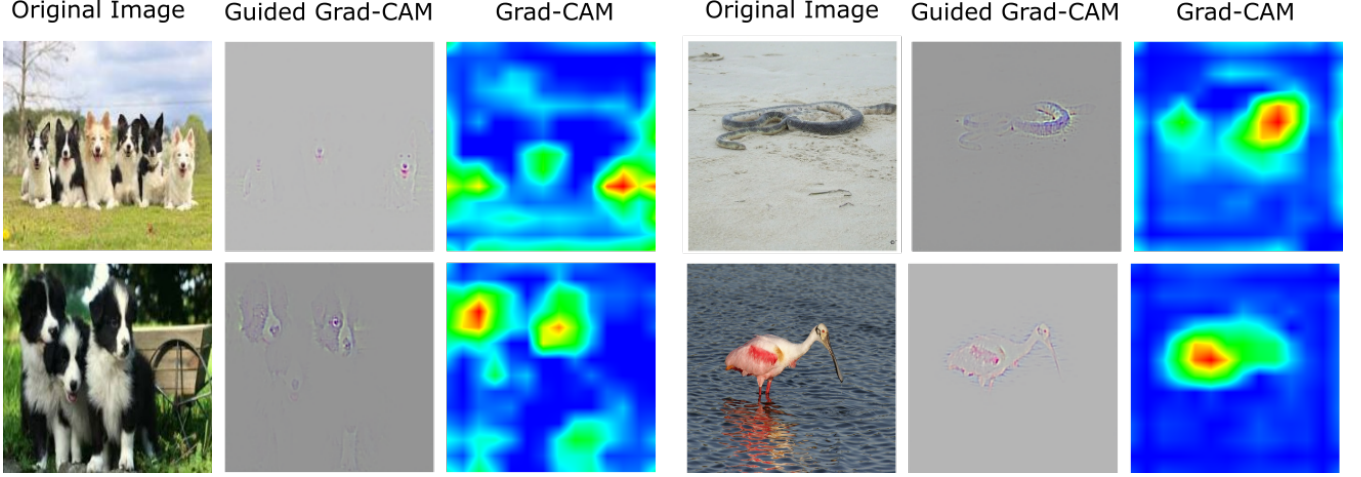


Fig. 1. Weaknesses of Grad-CAM: (a) multiple occurrences of the same class (Columns 1-3), and (b) localization capability of an object in an image (Columns 4-6). Note: All dogs are not visible for the first image under column 1. Full portion of the dogs are not visible for the second image under column 1. Both the classes are not visible in entirety under column 4 (part's of the snake's body is obscured and the bird's legs are partly missing in the generated saliency maps).

causes a specific unit in a neural network to have a high activation, for visualizing the functionality of the unit. A more guided approach to synthesizing input images that maximally activate a neuron was proposed by Simonyan *et al.* in [10]. In this work, they generated class-specific saliency maps, by performing a gradient ascent in pixel space to reach a maxima. This synthesized image serves as a class-specific visualization and helped delve deeper inside a CNN.

More recently, Ribeiro *et al.* [11] introduced a method called LIME (Local Interpretable Model-Agnostic Explanations) which makes a local approximation to the complex decision surface of any deep model with simpler interpretable classifiers like sparse linear models or shallow decision trees. For every test point, analyzing the weights of the sparse linear model gives some intuition to the non-expert as to the relevance of that feature in that particular prediction. In another approach, Al-Shedivat *et al.* [12] proposed contextual explanation networks (CENs), a class of models that jointly learns to predict and explain its decision. Unlike the existing posthoc model-explanation tools, CENs combine deep networks with context-specific probabilistic models and construct explanations in the form of locally-correct hypotheses. Konam [13] developed an algorithm to detect specific neurons which are responsible for decisions taken by a network and additionally locate patches of an input image which maximally activate those neurons. Lengerich *et al.* [14] proposed a different route towards explainability of CNNs. Instead of explaining the decision in terms of the input, they developed statistical metrics to evaluate the relation between the hidden representations in a network and its prediction. Another recent work [15], focusing on interpretability for self-driving cars, trained a visual attention model followed by a CNN model to obtain potentially salient image regions and applied causal filtering to find true input regions that actually influence the output.

In spite of the recent developments to make deep learning models explainable, we are far from the desired goal of interpretable deep learning models. There is continued

need to develop algorithms that can generate interpretable explanations of the results of deep models used across domains, which can then be investigated upon failures to make them more robust. Another important reason is to build trust in these systems for their proper integration into our daily lives.

Our work in this paper is mainly inspired by two algorithms, namely CAM [2] and Grad-CAM [6], which are widely used today [16]. Both CAM and Grad-CAM base their method on a fundamental assumption that the final score Y^c for a particular class c can be written as a linear combination of its global average pooled last convolutional layer feature maps A^k .

$$Y^c = \sum_k w_k^c \cdot \sum_i \sum_j A_{ij}^k \quad (1)$$

Each spatial location (i, j) in the class-specific saliency map L^c is then calculated as:

$$L_{ij}^c = \sum_k w_k^c \cdot A_{ij}^k \quad (2)$$

L_{ij}^c directly correlates with the importance of a particular spatial location (i, j) for a particular class c and thus functions as a visual explanation of the class predicted by the network. CAM estimates these weights w_k^c by training a linear classifier for each class c using the activation maps of the last convolutional layer generated for a given image. CAM however has some limitations. Its explainability prowess is limited to CNNs with a Global Average Pooling (GAP) penultimate layer, and requires retraining of multiple linear classifiers (one for each class), after training of the initial model.

Grad-CAM was built to address these issues. In their paper [6], the authors show that with this assumption (Eq. 1), the weights w_k^c for a particular feature map A^k and class c is equal to:

$$w_k^c = Z \cdot \frac{\partial Y^c}{\partial A_{ij}^k} \quad \forall \{i, j | i, j \in A^k\} \quad (3)$$

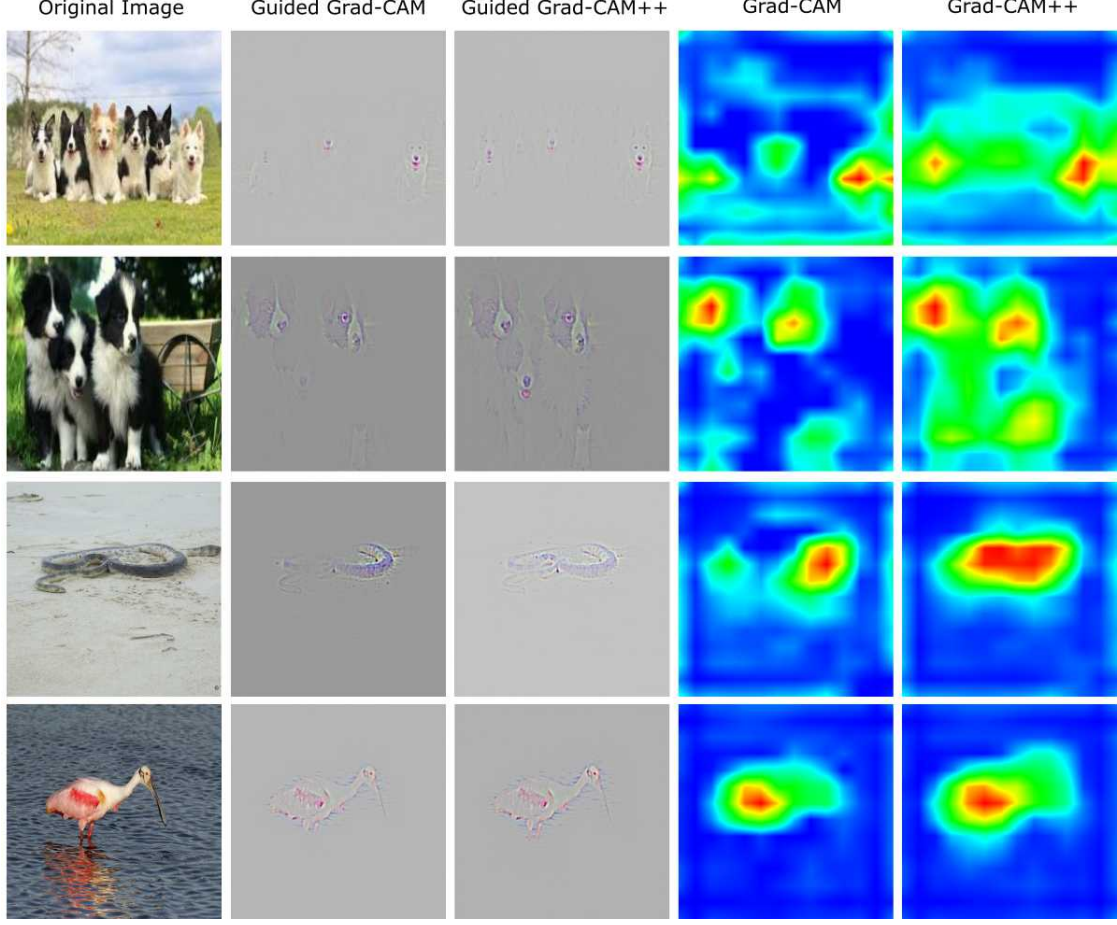


Fig. 2. Success of Grad-CAM++ for: (a) multiple occurrences of the same class (Rows 1-2), and (b) localization capability of an object in an image (Rows 3-4). Note: All dogs are better visible with more coverage, shown in the heatmap as well as Guided Grad-CAM++ for input images of rows 1 and 2. Full region of the class is visible for input images of rows 3 and 4 (full body of the snake and the head/legs of the bird).

where Z is a constant (number of pixels in the activation map). This helps in generalizing CAM to any deep architecture with a CNN block, without any retraining or architectural modification, where the final Y^c is a differentiable function of the activation maps A^k . However, this formulation (Eq. 3) makes the weights w_k^c independent of the positions (i, j) of a particular activation map A^k . The authors work around this limitation by taking a global average pool of the partial derivatives $\frac{\partial Y^c}{\partial A_{ij}^k}$, i.e.

$$w_k^c = \frac{1}{Z} \sum_i \sum_j \frac{\partial Y^c}{\partial A_{ij}^k} \quad (4)$$

To obtain fine-grained pixel-scale representations, the proposers of Grad-CAM upsample and fuse their class-specific saliency map L^c via point-wise multiplication with the visualizations generated by Guided Backpropagation. This visualization is referred to as Guided Grad-CAM. This approach however has some shortcomings as illustrated in Fig. 1. Grad-CAM fails to properly localize objects in an image if the image contains multiple occurrences of the same class. This is a serious issue as multiple occurrences of the same object in an image is a very common occurrence in the real world. Another consequence of an unweighted average of partial derivatives is that often, the localization doesn't

correspond to the entire object, but bits and parts of it. This can hamper the user's trust in the model, and impede Grad-CAM's premise of making a deep CNN more transparent.

In this manuscript, we propose a generalization to Grad-CAM which addresses the abovementioned issues and consequently serves as a better explanation algorithm for a given CNN architecture, and hence the name for the proposed method, Grad-CAM++. We formally derive closed-form solutions for the proposed method and carefully design experiments to evaluate the competence of Grad-CAM++ both objectively and subjectively. In all the experiments, Grad-CAM was used as a *baseline* comparison method as it is considered the current state-of-the-art CNN discriminative (class specific saliency maps) visualization technique [16].

3 GRAD-CAM++ METHODOLOGY

Building upon the gradient-based visualization techniques in Grad-CAM and CAM, we propose a generalized method called Grad-CAM++, which is formulated by explicitly modeling the contributions of each pixel in the feature maps of a CNN to the final output. In particular, we reformulate Eq. 1 by explicitly coding the structure of the weights w_k^c as:

$$w_k^c = \sum_i \sum_j \alpha_{ij}^{kc} \text{relu}\left(\frac{\partial Y^c}{\partial A_{ij}^k}\right) \quad (5)$$

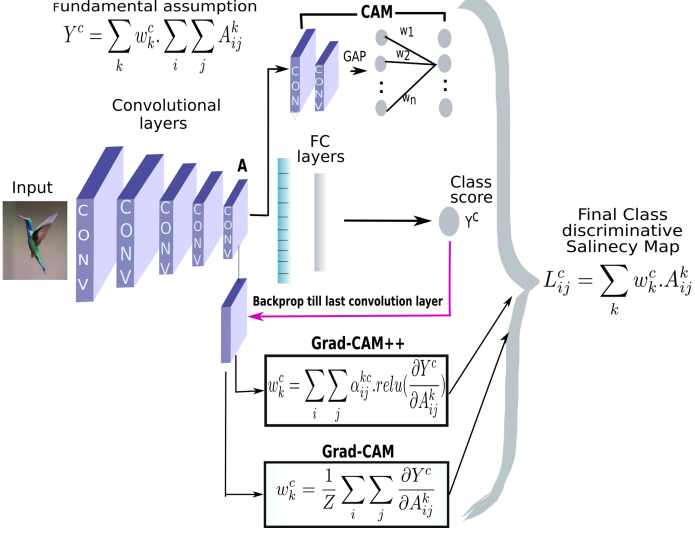


Fig. 3. An overview of all the three methods – CAM, Grad-CAM, Grad-CAM++ – with their respective computation expressions.

where $relu$ is the Rectified Linear Unit activation function. The idea behind this formulation is that w_k^c captures the importance of a particular activation map A^k . Previous works in pixel-space visualization like Deconvolution [1] and Guided Backpropagation [7] have shown the importance of positive gradients in producing saliency maps for a particular convolutional layer. A positive gradient at location (i, j) for an activation map A^k implies that increasing intensity of pixel (i, j) would have a positive influence over the class score Y^c . Thus, a linear combination of the positive partial derivatives w.r.t. each pixel in an activation map A^k would capture the importance of that map for class c . This structure ensures that the weights w_k^c are a weighted average of the gradients as opposed to a global average (Eq. 4). An empirical verification of this “positive gradients” hypothesis is presented later in Section 7.

We now formally derive a method for obtaining the gradient weights α_{ij}^{kc} for a particular class c and activation map k . Let Y^c be the score of a particular class c . Combining Eq. 1 and Eq. 5, we get:

$$Y^c = \sum_k [\sum_i \sum_j \{\sum_a \sum_b \alpha_{ab}^{kc} \cdot relu(\frac{\partial Y^c}{\partial A_{ab}^k})\} A_{ij}^k] \quad (6)$$

Here, (i, j) and (a, b) are iterators over the same activation map A^k . Without loss of generality, we drop the $relu$ as it only functions as a threshold for allowing the gradients to flow back. Taking partial derivative w.r.t. A_{ij}^k on both sides:

$$\frac{\partial Y^c}{\partial A_{ij}^k} = \sum_a \sum_b \alpha_{ab}^{kc} \cdot \frac{\partial Y^c}{\partial A_{ab}^k} + \sum_a \sum_b A_{ab}^k \{\alpha_{ij}^{kc} \cdot \frac{\partial^2 Y^c}{\partial A_{ij}^k \partial A_{ij}^k}\} \quad (7)$$

Taking partial derivative w.r.t. A_{ij}^k on both sides:

$$\frac{\partial^2 Y^c}{\partial A_{ij}^k \partial A_{ij}^k} = 2 \cdot \alpha_{ij}^{kc} \cdot \frac{\partial^2 Y^c}{\partial A_{ij}^k \partial A_{ij}^k} + \sum_a \sum_b A_{ab}^k \{\alpha_{ij}^{kc} \cdot \frac{\partial^3 Y^c}{\partial A_{ij}^k \partial A_{ij}^k \partial A_{ij}^k}\} \quad (8)$$

Rearranging terms, we get:

$$\alpha_{ij}^{kc} = \frac{\frac{\partial^2 Y^c}{\partial A_{ij}^k \partial A_{ij}^k}}{2 \frac{\partial^2 Y^c}{\partial A_{ij}^k \partial A_{ij}^k} + \sum_a \sum_b A_{ab}^k \{\frac{\partial^3 Y^c}{\partial A_{ij}^k \partial A_{ij}^k \partial A_{ij}^k}\}} \quad (9)$$

If $\forall i, j$, $\alpha_{ij}^{kc} = Z^{-1}$, Grad-CAM++ reduces to the formulation for Grad-CAM (Eq. 4) Thus, Grad-CAM++, as its name suggests, is a generalized formulation of Grad-CAM. In principle, the class score Y^c can be any prediction (object identification, classification, annotation, etc. to name a few); the only constraint being that Y^c must be a smooth function. For this reason, unlike Grad-CAM (which takes the penultimate layer representation as their class score Y^c), we pass the penultimate layer scores through an exponential function, as the exponential function is infinitely differentiable. The time overhead for calculating higher-order derivatives would be of the same order as Grad-CAM, as only the diagonal terms are used (no cross higher-order derivatives). If we pass the penultimate layer scores through an exponential function and the network architecture between the final convolutional layer and the penultimate layer has only linear or ReLU activation functions, the calculation of higher-order derivatives becomes trivial. Let S^c be the penultimate layer scores for class c .

$$Y^c = \exp(S^c) \quad (10)$$

$$\frac{\partial Y^c}{\partial A_{ij}^k} = \exp(S^c) \frac{\partial S^c}{\partial A_{ij}^k} \quad (11)$$

The quantity $\frac{\partial S^c}{\partial A_{ij}^k}$ can be easily calculated using machine learning libraries such as PyTorch or TensorFlow, which implement automatic differentiation.

$$\frac{\partial^2 Y^c}{(\partial A_{ij}^k)^2} = \exp(S^c) \left[\left(\frac{\partial S^c}{\partial A_{ij}^k} \right)^2 + \frac{\partial^2 S^c}{(\partial A_{ij}^k)^2} \right] \quad (12)$$

Now, assuming a ReLU activation function, $f(x) = \max(x, 0)$, its derivatives are given by:

$$\begin{aligned} \frac{\partial f(x)}{\partial x} &= 1 & x > 0 \\ &= 0 & x \leq 0 \end{aligned} \quad (13)$$

$$\frac{\partial^2 f(x)}{\partial x^2} = 0 \quad (14)$$

Eq. 14 holds even if the activation function is linear. Inserting Eq. 14 into Eq. 12, we have:

$$\frac{\partial^2 Y^c}{(\partial A_{ij}^k)^2} = \exp(S^c) \left(\frac{\partial S^c}{\partial A_{ij}^k} \right)^2 \quad (15)$$

Similarly,

$$\frac{\partial^3 Y^c}{(\partial A_{ij}^k)^3} = \exp(S^c) \left(\frac{\partial S^c}{\partial A_{ij}^k} \right)^3 \quad (16)$$

Inserting Eq. 15 and Eq. 16 into Eq. 9, we get:

$$\alpha_{ij}^{kc} = \frac{(\frac{\partial S^c}{\partial A_{ij}^k})^2}{2(\frac{\partial S^c}{\partial A_{ij}^k})^2 + \sum_a \sum_b A_{ab}^k (\frac{\partial S^c}{\partial A_{ij}^k})^3} \quad (17)$$

So, with a single backward pass on the computational graph, all the gradient weights α_{ij}^{kc} (as originally defined in Eq. 5) can be computed. We used the exponential function due to its simplicity. Other smooth functions such as the softmax activation function can also be used with corresponding closed-form expressions to compute the weights.

The derivation of the gradient weights for softmax is given in Section 3.1.

The class-discriminative saliency maps for a given image, L^c is then calculated as a linear combination of the forward activation maps, followed by a *relu* layer. Each spatial element in the saliency map L^c is then computed as:

$$L_{ij}^c = \text{relu}\left(\sum_k w_k^c \cdot A_{ij}^k\right) \quad (18)$$

To generate class-discriminative saliency maps along with the richness of pixel-space gradient visualization methods, we pointwise multiply the upsampled (to image resolution) saliency map L^c with the pixel-space visualization generated by Guided Backpropagation. This technique is reminiscent to the technique adopted by Grad-CAM. The representations thus generated are called Guided Grad-CAM++.

In Fig. 2, we illustrate visually how taking a weighted combination of positive partial derivatives (Eq. 5) instead of a global average (Eq. 4) addresses the problem of identifying multiple occurrences of the same class in an image and improper object localization. A bird’s eye view of all the three methods – CAM, Grad-CAM, and Grad-CAM++ – is presented in Fig. 3.

3.1 Gradient weights for the softmax function

In Section 3, we derived closed-form solutions for the gradient weights α_{ij}^{kc} for a particular feature map k , class c and spatial location i, j . Like the exponential function, the softmax function is also smooth and commonly employed to obtain final class probabilities in classification scenarios. In this case, the final class score Y^c is –

$$Y^c = \frac{\exp(S^c)}{\sum_k \exp(S^k)} \quad (19)$$

where, the index k runs over all the output classes and S^k refers to the score pertaining to output class k of the penultimate layer.

$$\frac{\partial Y^c}{\partial A_{ij}^k} = Y^c \left[\frac{\partial S^c}{\partial A_{ij}^k} - \sum_k Y^k \frac{\partial S^k}{\partial A_{ij}^k} \right] \quad (20)$$

If the neural network has just linear or ReLU activation functions then $\frac{\partial^2 S^c}{(\partial A_{ij}^k)^2}$ would be 0 (Eq. 14 in main text).

$$\begin{aligned} \frac{\partial^2 Y^c}{(\partial A_{ij}^k)^2} &= \frac{\partial Y^c}{\partial A_{ij}^k} \left[\frac{\partial S^c}{\partial A_{ij}^k} - \sum_k Y^k \frac{\partial S^k}{\partial A_{ij}^k} \right] \\ &\quad - Y^c \left(\sum_k \frac{\partial Y^k}{\partial A_{ij}^k} \frac{\partial S^k}{\partial A_{ij}^k} \right) \end{aligned} \quad (21)$$

$$\begin{aligned} \frac{\partial^3 Y^c}{(\partial A_{ij}^k)^3} &= \frac{\partial^2 Y^c}{(\partial A_{ij}^k)^2} \left[\frac{\partial S^c}{\partial A_{ij}^k} - \sum_k Y^k \frac{\partial S^k}{\partial A_{ij}^k} \right] \\ &\quad - 2 \frac{\partial Y^c}{\partial A_{ij}^k} \left(\sum_k \frac{\partial Y^k}{\partial A_{ij}^k} \frac{\partial S^k}{\partial A_{ij}^k} \right) - Y^c \left(\sum_k \frac{\partial^2 Y^k}{(\partial A_{ij}^k)^2} \frac{\partial S^k}{\partial A_{ij}^k} \right) \end{aligned} \quad (22)$$

Plugging Eq. 21 and Eq. 22 in Eq. 9 (in the main text) the gradient weights can be obtained. Although, evaluating the gradient weights in the case of the softmax function is more involved than the case of the exponential function, it can still be computed via a single backward pass on the computation graph for computing the $\frac{\partial S^k}{\partial A_{ij}^k}$ terms.



Fig. 4. Example explanation maps for 2 images generated by Grad-CAM++ and Grad-CAM.

4 EMPIRICAL EVALUATION OF GENERATED EXPLANATIONS

A good explanation must be consistent with the model prediction (faithfulness) and display results in a human interpretable format (human trust). In addition to the visual results shown in Fig. 2, we also conducted other experiments to evaluate our method, Grad-CAM++, both objectively (faithfulness) and subjectively (human trust). We now present these experiments and results in this section. For all experiments, we used an off-the-shelf VGG-16 [17] model from the Caffe Model Zoo [18], to be consistent with earlier work that used the same model [6]. We also show results with AlexNet [19] and ResNet-50 [20] architectures in the Appendix. Implementation of our method is available at https://github.com/adityac94/Grad_CAM_plus_plus.

4.1 Objective Evaluation of Performance based on Object Recognition

In this section, we evaluate the faithfulness of the explanations generated by Grad-CAM++ over PASCAL VOC 2007 val set. We choose this dataset in particular as it contains images with multiple classes. For every image, a corresponding explanation map E^c is generated by point-wise multiplication of the class-discriminative saliency maps (upsampled to image resolution) with the original image:

$$E^c = L^c \circ I \quad (23)$$

where \circ refers to a Hadamard product, I refers to the input image and L^c is the class-discriminative saliency maps as defined in Eq. 18. The class c used in the experiments for each image was the class predicted by the model. This was done for both the E^c s generated from Grad-CAM++ and Grad-CAM. Some example explanation maps are shown in Fig. 4. The explanation maps occlude parts of the image according to their importance in model decision-making as determined by the corresponding method (Grad-CAM++/Grad-CAM). Our experimental setup consists of three different metrics: (i) Average drop %; (ii) % increase in confidence; and (iii) Win %.

(i) Average Drop %: A good explanation map for a class should highlight the regions that are most important. A deep CNN model looks for different patterns in the entire image space before making a decision. Occluding parts of an image would mostly lower the confidence of the model in its decision (as opposed to the entire image). However, as the explanation maps keep the most important regions for a particular class in an image intact, this fall is expected to be less when occluding the unimportant regions alone. This metric compares the average % drop in the model’s confidence for a particular class in an image after occlusion. For example, let’s say the model predicted an object Tiger in an image with confidence 0.8. When shown the explanation map for the same image, if the model’s confidence in the class Tiger fell to 0.4, the % drop in model confidence would be 50%. This value is computed per image and averaged over the entire dataset. Formally, the Average Drop % is expressed as $(\sum_{i=1}^N \frac{\max(0, Y_i^c - O_i^c)}{Y_i^c})100$. The summation is over all the images in the dataset. Y_i^c refers to the model’s output score (confidence) for class c for the i^{th} image and O_i^c refers to the same model’s confidence in class c with the unimportant regions of the i^{th} input image occluded. The \max function in the numerator ensures a 0 contribution to the Average Drop % for input images where $O_i^c > Y_i^c$ (refer to the % Increase in Confidence metric).

(ii) % Increase in Confidence: Complementary to the previous metric, it is often possible that the entirety of patterns the deep CNN looks for is in the most discriminative part highlighted by the explanation maps. In this scenario, one would expect an increase in the model’s confidence for that particular class, at least on certain input images, when the unimportant regions are occluded. This metric measures the number of times in the entire dataset, the model’s confidence increased upon occluding unimportant regions. This value is expressed as a percentage. Formally, the % Increase in Confidence is expressed as $(\sum_{i=1}^N \frac{\mathbb{1}_{Y_i^c < O_i^c}}{N})100$. $\mathbb{1}_x$ is the indicator function which evaluate to 1 if the constraint x is satisfied. All other notations are as defined in the previous paragraph (refer to the Average Drop % metric).

(iii) Win %: While the first two metrics (Average drop% and % increase in confidence) evaluate the capability of an explanation map in highlighting the influential regions of an image, the win % metric explicitly compares the contrastive effectiveness of the explanation maps generated by Grad-CAM++ and Grad-CAM. It measures the number of times in a given set of images, the fall in the model’s confidence for an explanation map generated by Grad-CAM++ is less than the respective explanation map generated by Grad-CAM. This value is expressed as a percentage. A lower fall would indicate that the salient features of an image preserved by Grad-CAM++ explanation map are more *model-appropriate* than the respective salient features captured by the Grad-CAM explanation map.

The results of our experiments on the ImageNet (ILSVRC2012) validation dataset are shown in Table 1. Grad-CAM++ performs better than Grad-CAM in all three metrics. A higher % increase in confidence and a lower

Method	Grad-CAM++	Grad-CAM
Average Drop % (Lower is better)	36.84	46.56
% Incr. in Confidence (Higher is better)	17.05	13.42
Win % (Higher is better)	70.72	29.28

TABLE 1
Results for objective evaluation of the explanations generated by Grad-CAM++ and Grad-CAM on the ImageNet (ILSVRC2012) validation set (“incr” denotes increase). The results point to the improved performance of the proposed Grad-CAM++ method.

Method	Grad-CAM++	Grad-CAM
Average Drop % (Lower is better)	19.53	28.54
% Incr. in Confidence (Higher is better)	18.96	21.43
Win % (Higher is better)	61.47	39.44

TABLE 2
Results for objective evaluation of the explanations generated by both Grad-CAM++ and Grad-CAM on the PASCAL VOC 2007 validation set (“incr” denotes increase).

average drop % is consistent with our hypothesis that re-formulating the weights as Eq. 5 helps in better localizing the most discriminative regions of an image (for a particular class c) as compared to global average pooling of the gradients (Eq. 4).

We also performed the same experiment on the Pascal VOC 2007 validation set. The Pascal VOC 2007 dataset is a multi-label setting where a particular image might contain objects belonging to multiple classes. The rationale behind this setup was to evaluate the performance when there are multiple objects in an image. The results for this experiment are shown in Table 2, which once again supports the superior performance of Grad-CAM++ on datasets with multiple objects. In this case, the Pascal VOC 2007 train set was used to fine-tune the VGG-16 network (trained on ImageNet). More empirical results showing the effectiveness of Grad-CAM++ for other CNN architectures, viz, AlexNet [19] and Resnet-50 [20] are discussed in Appendix A.1 and A.2.

4.2 Evaluating Human Trust

The explainability prowess of any algorithm for a given deep model depends on two important factors - *faithfulness* and human trust or *interpretability*. In the previous subsection, we explored “faithfulness”; here, we evaluate the “interpretability” of our explanations. We generated explanation maps for all images in the ImageNet validation set for 5 classes, leading to a total of 250 images. The explanations generated by Grad-CAM were treated as baseline for comparison. These maps, along with their corresponding original image, were shown to 13 human subjects (who have no knowledge of deep learning whatsoever) and asked which explanation algorithm invoked more trust in the underlying model. Thus, the explanation algorithm that gets more votes from the subjects can be considered as doing a better job of invoking human trust in the underlying VGG-16 model. (The assumption in this work is that a pre-trained

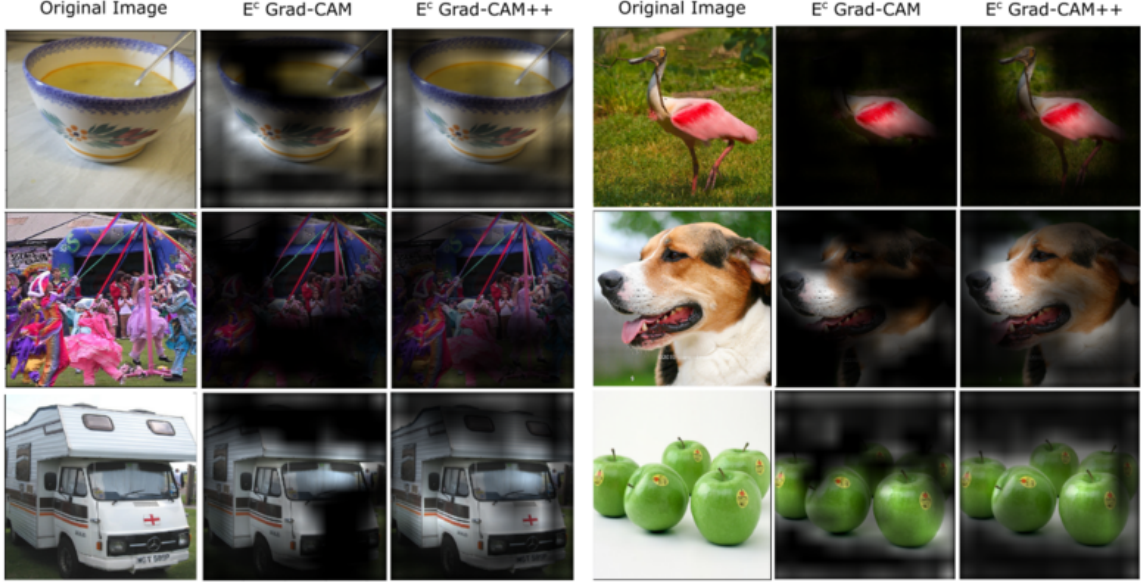


Fig. 5. Explanation maps for sample images from ImageNet generated by Grad-CAM and Grad-CAM++.

VGG-16 network [17] has learnt the hidden representations of the object categories adequately.) To further substantiate our claim, we chose 5 classes which have the highest F1-score for the validation dataset (above 0.94). As each class just has 50 images in the validation set, F1-score (which is the harmonic mean of precision and recall) is a better suited metric than classification error.

For each image, two explanation maps were generated, one from Grad-CAM and one from Grad-CAM++. Some visual examples of these explanation maps are presented in Fig. 5. The subjects were provided the class of the image and asked to select the map they felt best described the object in the image (with no knowledge of which one is Grad-CAM or Grad-CAM++). The subjects also had the option to select “same” if they felt both the generated explanation maps were similar. The responses for each image was normalized, such that the total score possible for each image is 1.0. To elaborate on this point, we obtained 13 responses for each image. For example, among the 13 responses, if 5 chose the explanation map generated by Grad-CAM++, 4 chose the explanation map generated by Grad-CAM and 4 chose the option “same”, the respective scores from Grad-CAM++ and Grad-CAM would be 0.38 and 0.31 (with the remaining being “same”). These normalized scores were then added. So, the total achievable score is 250. Grad-CAM++ achieved a score of **109.69** as compared to **56.08** of Grad-CAM. The remaining 84.23 was characterized as “same” by the human subjects. This empirical study provides strong evidence for our hypothesis that weighing the partial derivatives (Eq. 5) helps in more human-interpretable image localization, and thus invokes a greater trust in the deep model that makes the decision. As Grad-CAM++ is a generalization of Grad-CAM, it performs similar to Grad-CAM in about 33.69% cases.

4.3 Harnessing Explainability to generate Object Localizations

In this subsection, we show the effectiveness of Grad-CAM++ for class-discriminative localization of objects in a given image. We selected Pascal VOC 2012 dataset for this experiment as it has bounding box annotations for each of its image, and is also multi-label. The VGG-16 network was fine-tuned on the VOC 2012 train set and evaluations were done using the VOC 2012 validation set. For a given image and a class c , the corresponding explanation map $E^c(\delta)$ is generated using Eq. 23, with a slight modification that the class-specific saliency maps L^c s are min-max normalized and thresholded by a particular intensity value δ . All intensities above δ were converted to 1.0. We define an Intersection over Union (IoU) metric $Loc_I^c(\delta)$, for a particular class c , threshold value δ and an image I , as below:

$$Loc_I^c(\delta) = \frac{\text{Area}(\text{internal pixels})}{\text{Area}(\text{bounding box}) + \text{Area}(\text{external pixels})} \quad (24)$$

where, $\text{Area}(\text{bounding box})$ refers to the area of the bounding box/es for a particular class c and a given image I , $\text{Area}(\text{internal pixels})$ refers to the number of non-zero pixels in the explanation map that lie inside the bounding box/es and $\text{Area}(\text{external pixels})$ refers to the number of non-zero pixels that lie outside the bounding box/es. Higher the value of $Loc_I^c(\delta)$, better the localization of the explanation map. We only considered those images in the VOC 2012 val set, which contained bounding box annotations for at least one class in the predicted Top-5 classes by the VGG-16 network. The results for this experiment are tabulated in Table 3. We note that the same δ was used to threshold both explanation maps (Grad-CAM++ and Grad-CAM) for fairness of comparison. The results are, once again, in favor of the performance of Grad-CAM++. We also illustrate visual examples of the improved object localization obtained by the proposed method in Fig. 6.

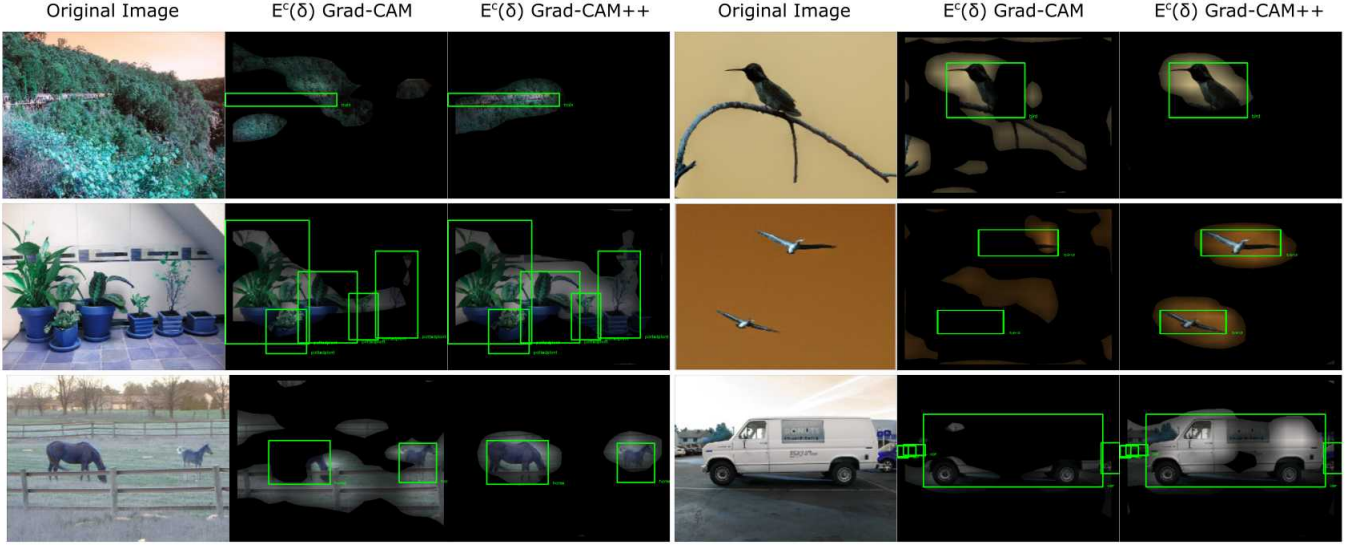


Fig. 6. Some visual examples depicting the object localization capabilities of both Grad-CAM and Grad-CAM++. The results are for $E^c(\delta = 0.25)$. The green boxes represent ground truth annotations for the images.

Method	Grad-CAM++	Grad-CAM
$mLoc_I^c(\delta = 0)$	0.34	0.33
$mLoc_I^c(\delta = 0.25)$	0.38	0.28
$mLoc_I^c(\delta = 0.5)$	0.28	0.16

TABLE 3

Results for objective evaluation of performance based on object localization by both Grad-CAM++ and Grad-CAM on the PASCAL VOC 2012 val set. These results highlight the better object localization property of Grad-CAM++. Here $mLoc_I^c(\delta = \eta)$ refers to mean $Loc_I^c(\delta)$ per label per image, with a threshold value of $\delta = \eta$ (Higher is better).

5 LEARNING FROM EXPLANATIONS: KNOWLEDGE DISTILLATION

Human-interpretable deep learning models can potentially serve as pedagogical agents and extend the frontiers of human knowledge, although a distant dream as things stand today. Inspired by the ideas introduced by Zagoruyko and Komodakis [21], we show that in a constrained teacher-student learning setting [22]–[25], knowledge transfer to a shallow student (commonly called *knowledge distillation*) is possible from the explanation of CNN decisions generated by Grad-CAM++. For the first experiment, we use Wide Resnets [26] for both the student and teacher networks. We train a WRN-40-2 teacher network (2.2 M parameters) on the CIFAR-10 [27] dataset. In order to train a student WRN-16-2 network (0.7 M parameters), we introduce a modified loss $L_{exp_student}$, which is a weighted combination of the standard cross entropy loss L_{cross_ent} and an *interpretability loss*, $L_{interpret}$:

$$L_{exp_student}(c, W_s, W_t, I) = L_{cross_ent}(c, W_s(I)) + \alpha(L_{interpret}(c, W_s, W_t, I)) \quad (25)$$

where $L_{interpret}$ is defined as:

$$L_{interpret}(c, W_s, W_t, I) = \|L_s^c(W_s(I)) - L_t^c(W_t(I))\|_2^2 \quad (26)$$

In the above equations, I refers to the input image and c denotes the corresponding output class label. L^c is as

defined in Eq. 18 and α is a hyper parameter which controls the amount of weight given to the interpretability loss. W_i refers to the weights of the i network. The subscripts s and t refer to the student and teacher networks respectively. The intuition behind the formulation in Eq. 25 is that the student network should not only try to match its output probabilities with the actual ground truth labels but also learn the relevant parts of a given image for making a particular decision (the $L_{interpret}$ term) from the teacher network.

Table 4 shows the results for this experiment. $L_{exp_student}(\text{Grad-CAM++})$ and $L_{exp_student}(\text{Grad-CAM})$ refer to loss functions as defined in Eq. 25, where the saliency maps are generated for a given image I using Grad-CAM++ and Grad-CAM respectively. L_{KD} is the knowledge distillation loss introduced by Hinton *et al.*[22] with temperature parameter set to 4 (same as used in [21]). By transferring the salient features responsible for a CNN’s decision in the teacher network, our experiments show it is possible to train a much shallower student network (a 68.18% reduction in the number of parameters) to achieve a lower test error rate of 5.56% as compared to the teacher’s error rate of 5.8%. As already established in Section 4.1, Grad-CAM++ provides explanations that are more faithful to the underlying deep model than Grad-CAM, which also explains the better performance of Grad-CAM++ for explanation-based knowledge distillation.

To further study the potential of knowledge distillation using Grad-CAM++, we conducted experiments (with $L_{exp_student}$) on the PASCAL VOC 2007 data set, and the results are shown in Table 5. In the CIFAR-10 dataset, each image is of size 32×32 , allowing very little spatial bandwidth for transfer of salient features [21]. However, the VOC 2007 data set has larger images with bigger spatial extents of the prominent pixels for a CNN’s decision. The results, resulting in an increase in the mean Average Precision (mAP) of about 35% as compared to training the student network solely on the VOC 2007 train set. The teacher network is a

loss function used	test error rate
L_{cross_ent}	6.78
$L_{exp_student}$(Grad-CAM++)	6.74
$L_{exp_student}$ (Grad-CAM)	6.86
$L_{cross_ent} + L_{KD}$	5.68
$L_{exp_student}$(Grad-CAM++)+L_{KD}	5.56
$L_{exp_student}$ (Grad-CAM)+ L_{KD}	5.8

TABLE 4

Comparative results for student (WRN-16-2) learning from explanations of a deeper teacher network (WRN-40-2), produced using Grad-CAM++ and Grad-CAM. The results indicate that an improved performance is possible if the interpretability of the teacher network (the output of Grad-CAM++) is utilized in the optimization formulation of the shallower student network (see results marked in bold). L_{cross_ent} is the normal cross entropy loss function, i.e. the student network is trained independently on the dataset without any intervention from the expert teacher.

loss function used	mAP (% increase)
$L_{exp_student}$(Grad-CAM++)	0.42 (35.5%)
$L_{cross_ent} + L_{KD}$	0.34 (9.7%)
L_{cross_ent} [Baseline]	0.31 (0.0%)

TABLE 5

Results for training a student network with explanations from the teacher (VGG-16 fine-tuned) and with knowledge distillation on PASCAL VOC 2007 dataset. The results show that a much higher improvement in the performance of the student network is possible when using interpretability loss from Grad-CAM++ as compared to just using knowledge distillation. L_{cross_ent} is the normal cross entropy loss function, i.e. the student network is trained independently on the dataset without any intervention from the expert teacher. The % increase is with respect to the baseline loss L_{cross_ent} .

standard VGG-16 architecture pretrained on Imagenet with the penultimate layer fine-tuned to the VOC 2007 train set. The student networks consists of a shallower 11-layer CNN network with 27M parameters (an 80% reduction). (The α parameter in Eq. 25 was taken to be 0.01 for all experiments illustrated in this section).

6 EXPLANATIONS FOR IMAGE CAPTIONING AND 3D ACTION RECOGNITION TASKS

Similar to other such methods, Grad-CAM++ can be used to understand any machine learning model’s decision as long as it utilizes a CNN as an integral module. In this section, we present the results for experiments on two such tasks - Image Captioning and 3D Action Recognition. To the best of our knowledge, this is the first time visual explanations of CNNs in the video domain has been explored.

6.1 Image Captioning

We considered a standard image captioning model [28] trained on the Flickr30k data set [29] [30] using an adaptation of the popular Show-and-Tell model [31]. The basic architecture involves a CNN to encode the image followed by an LSTM to generate the captions. For fairness of comparison, we use the same settings as used for this task in Grad-CAM. Fig. 7 illustrates the salient features (heatmap) of four randomly chosen images from the Flickr30k data set, extracted using Grad-CAM and Grad-CAM++ for the predicted caption. In all the images, Grad-CAM++ produces superior heatmaps than Grad-CAM. For instance, in the first example, Grad-CAM++ correctly highlights both the girl

and the plant for the caption “A young girl accompanied by a small plant”, whereas Grad-CAM determines the girl to be the only deciding factor for the same above-said caption. In the second example in the first row, although the predicted caption is wrong, Grad-CAM++’s visualization gives insight into what the network focused on - the colored glasses (which can be interpreted as pillars by the network) and the man. Comparatively, Grad-CAM’s visualization is incomplete with no heat generated at the man’s spatial location in the image. For generating the heatmaps, Eq. 18 was used with the log probability of the predicted caption as Y^c (for classification tasks, Y^c was related to the output of the neuron representing the c^{th} class).

6.2 3D Action Recognition

For the task of 3D action recognition, we used a 3D-CNN architecture (standardized for video recognition tasks). We used the C3D model [32], pretrained on the Sports-1M Dataset [33] containing 1,133,158 YouTube sports videos which have been annotated with 487 Sports labels. The saliency maps are generated from the last convolution layer feature maps of the C3D model. The generated saliency maps (for both Grad-CAM and Grad-CAM++) were upsampled to the video resolution and then the corresponding explanation video maps were generated by point-wise multiplication with the original video. While generating the explanation maps E^c as in Eq. 23, I is the input video in this case and c is the predicted action of the video. Sample qualitative results with randomly chosen sample sports videos (no handpicking was done while choosing these videos) are shown in the Appendix A.3. The generated video explanation maps, E^c s, show clearer depiction of salient features for the corresponding action in the case of Grad-CAM++ as compared to Grad-CAM.

7 WHY ONLY POSITIVE GRADIENTS IN GRAD-CAM++?

We hypothesize in this work that a weighted combination of positive gradients w.r.t. each pixel in an activation map A^k strongly correlates with the importance of that activation map for a given class c (Eq. 5 in Section 3). In this section, we test the correctness of this assumption by relaxing the constraint on the gradients. We take the same VGG-16 model used for our objective evaluation studies on the Pascal VOC 2007 val set (Section 4.1) and redo the experiment with a slightly different w_k^c :

$$w_k^c = \sum_i \sum_j \alpha_{ij}^{kc} \cdot \frac{\partial Y^c}{\partial A_{ij}^k} \quad (27)$$

Note that the `relu()` function is dropped as we consider all the gradients. The α_{ij}^{kcs} are calculated as in Eq. 9, with the exception that $\alpha_{ij}^{kc} \neq 0$ for negative gradients.

$$\alpha_{ij}^{kc} = \frac{\frac{\partial^2 Y^c}{(\partial A_{ij}^k)^2}}{2 \frac{\partial^2 Y^c}{(\partial A_{ij}^k)^2} + \sum_a \sum_b A_{ab}^k \{ \frac{\partial^3 Y^c}{(\partial A_{ij}^k)^3} \}} \quad (28)$$

We refer to this modified version of Grad-CAM++ (where we do not restrict to positive gradients) as Grad-CAM++ $^\perp$. Table 6 shows the poor performance of Grad-CAM++ $^\perp$ when compared to Grad-CAM. These results

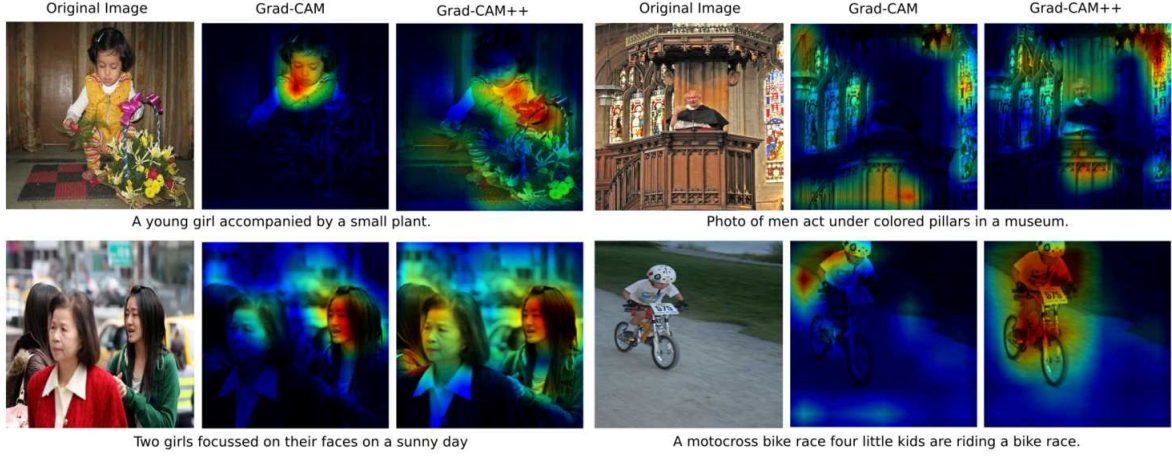


Fig. 7. Explanations of image captions predicted by CNN-based neural network architectures using both Grad-CAM and Grad-CAM++. All the examples show an improved visualization with Grad-CAM++.

strongly support our assumption that the positive gradients are critical to decide the importance of an activation map A^k for a given class c .

Method	Grad-CAM $^{++\perp}$	Grad-CAM
- Average drop% (Lower is better)	32.43	28.54
- % incr. in confidence (Higher is better)	19.12	21.43
- Win% (Higher is better)	26.09	73.91

TABLE 6

Results for objective evaluation of the explanations generated by $\text{Grad-CAM}^{++\perp}$ and Grad-CAM on the Pascal VOC 2007 validation set (2510 images) ("incr" denotes increase). In this experiment, the weights w_k^c 's were taken to be a weighed combination of all the gradients of an activation map A^k (both positive and negative).

8 CONCLUSION

In this work, we proposed a generalized class-discriminative approach for visual explanations of CNN based architectures, Grad-CAM++. We provide a formal derivation for our method and show that it is a simple, yet effective generalization of earlier gradient-based visual explanation methods. Our method addresses the shortcomings of Grad-CAM - multiple occurrences of same class in an image and poor object localizations. This was demonstrated via visual examples. We validated the effectiveness of our method both objectively (faithfulness to the model being explained) and subjectively (invoking human trust) using standard well-known CNN models and datasets (ImageNet and Pascal VOC). We showed that Grad-CAM++ can also prove superior on tasks such as image caption generation and video understanding (where ours is the first such work for visual explanations). In Section 5, we motivated a research direction where explanations of a deep network are not only used to understand the reasonings behind model decisions but also utilized to train a shallower student network. The student network learned much better representations than

the original teacher network (lower test error rate). Future work involves refining the loss formulation in the teacher-student setting so as to distill knowledge via Grad-CAM++ explanations more effectively. We also hope to explore the possibility of extending our algorithm to explain decisions made by other neural network architectures such as recurrent neural networks, long short-term memory networks, and generative adversarial networks.

ACKNOWLEDGMENTS

The authors would like to thank the Ministry of Human Resource Development, India for financial assistance and NVIDIA for donation of K40 GPU through their Academic Hardware Grant program.

REFERENCES

- [1] M. D. Zeiler and R. Fergus, "Visualizing and understanding convolutional networks," in *European conference on computer vision*. Springer, 2014, pp. 818–833.
- [2] B. Zhou, A. Khosla, A. Lapedriza, A. Oliva, and A. Torralba, "Learning deep features for discriminative localization," in *Proceedings of the IEEE Conference on Computer Vision and Pattern Recognition*, 2016, pp. 2921–2929.
- [3] M. Lin, Q. Chen, and S. Yan, "Network in network," *arXiv preprint arXiv:1312.4400*, 2013.
- [4] M. Oquab, L. Bottou, I. Laptev, and J. Sivic, "Is object localization for free? weakly-supervised learning with convolutional neural networks," in *Proceedings of the IEEE Conference on Computer Vision and Pattern Recognition*, 2015, pp. 685–694.
- [5] P. O. Pinheiro and R. Collobert, "From image-level to pixel-level labeling with convolutional networks," in *Proceedings of the IEEE Conference on Computer Vision and Pattern Recognition*, 2015, pp. 1713–1721.
- [6] R. R. Selvaraju, A. Das, R. Vedantam, M. Cogswell, D. Parikh, and D. Batra, "Grad-cam: Why did you say that? visual explanations from deep networks via gradient-based localization," *arXiv preprint arXiv:1610.02391*, 2016.
- [7] J. T. Springenberg, A. Dosovitskiy, T. Brox, and M. Riedmiller, "Striving for simplicity: The all convolutional net," *arXiv preprint arXiv:1412.6806*, 2014.
- [8] A. Mahendran and A. Vedaldi, "Salient deconvolutional networks," in *European Conference on Computer Vision*. Springer, 2016, pp. 120–135.
- [9] J. Yosinski, J. Clune, A. M. Nguyen, T. J. Fuchs, and H. Lipson, "Understanding neural networks through deep visualization," *CoRR*, vol. abs/1506.06579, 2015. [Online]. Available: <http://arxiv.org/abs/1506.06579>

- [10] K. Simonyan, A. Vedaldi, and A. Zisserman, "Deep inside convolutional networks: Visualising image classification models and saliency maps," *arXiv preprint arXiv:1312.6034*, 2013.
- [11] M. T. Ribeiro, S. Singh, and C. Guestrin, "Why should i trust you?: Explaining the predictions of any classifier," in *Proceedings of the 22nd ACM SIGKDD International Conference on Knowledge Discovery and Data Mining*. ACM, 2016, pp. 1135–1144.
- [12] M. Al-Shedivat, A. Dubey, and E. P. Xing, "Contextual explanation networks," *arXiv preprint arXiv:1705.10301*, 2017.
- [13] S. Konam, "Vision-based navigation and deep-learning explanation for autonomy," in *Masters thesis, Robotics Institute, Carnegie Mellon University, Pittsburgh, PA*, 2017.
- [14] B. J. Lengerich, S. Konam, E. P. Xing, S. Rosenthal, and M. Veloso, "Visual explanations for convolutional neural networks via input resampling," *arXiv preprint arXiv:1707.09641*, 2017.
- [15] J. Kim and J. Canny, "Interpretable learning for self-driving cars by visualizing causal attention," *arXiv preprint arXiv:1703.10631*, 2017.
- [16] K. Li, Z. Wu, K.-C. Peng, J. Ernst, and Y. Fu, "Tell me where to look: Guided attention inference network," *arXiv preprint arXiv:1802.10171*, 2018.
- [17] K. Simonyan and A. Zisserman, "Very deep convolutional networks for large-scale image recognition," *arXiv preprint arXiv:1409.1556*, 2014.
- [18] Y. Jia, E. Shelhamer, J. Donahue, S. Karayev, J. Long, R. Girshick, S. Guadarrama, and T. Darrell, "Caffe: Convolutional architecture for fast feature embedding," in *Proceedings of the 22nd ACM international conference on Multimedia*. ACM, 2014, pp. 675–678.
- [19] A. Krizhevsky, I. Sutskever, and G. E. Hinton, "Imagenet classification with deep convolutional neural networks," in *Advances in neural information processing systems*, 2012, pp. 1097–1105.
- [20] K. He, X. Zhang, S. Ren, and J. Sun, "Deep residual learning for image recognition," in *Proceedings of the IEEE conference on computer vision and pattern recognition*, 2016, pp. 770–778.
- [21] S. Zagoruyko and N. Komodakis, "Paying more attention to attention: Improving the performance of convolutional neural networks via attention transfer," *arXiv preprint arXiv:1612.03928*, 2016.
- [22] G. Hinton, O. Vinyals, and J. Dean, "Distilling the knowledge in a neural network," *arXiv preprint arXiv:1503.02531*, 2015.
- [23] A. Romero, N. Ballas, S. E. Kahou, A. Chassang, C. Gatta, and Y. Bengio, "Fitnets: Hints for thin deep nets," *arXiv preprint arXiv:1412.6550*, 2014.
- [24] B. B. Sau and V. N. Balasubramanian, "Deep model compression: Distilling knowledge from noisy teachers," *arXiv preprint arXiv:1610.09650*, 2016.
- [25] S. You, C. Xu, C. Xu, and D. Tao, "Learning from multiple teacher networks," in *Proceedings of the 23rd ACM SIGKDD International Conference on Knowledge Discovery and Data Mining*. ACM, 2017, pp. 1285–1294.
- [26] S. Zagoruyko and N. Komodakis, "Wide residual networks," *arXiv preprint arXiv:1605.07146*, 2016.
- [27] A. Krizhevsky, V. Nair, and G. Hinton, "The cifar-10 dataset," *online: http://www.cs.toronto.edu/kriz/cifar.html*, 2014.
- [28] R. Puri and D. Ricciardelli, "Caption this, with tensorflow," in *https://www.oreilly.com/learning/caption-this-with-tensorflow*, Accessed 28 March, 2017.
- [29] B. A. Plummer, L. Wang, C. M. Cervantes, J. C. Caicedo, J. Hockenmaier, and S. Lazebnik, "Flickr30k entities: Collecting region-to-phrase correspondences for richer image-to-sentence models," *IJCV*, vol. 123, no. 1, pp. 74–93, 2017.
- [30] P. Young, A. Lai, M. Hodosh, and J. Hockenmaier, "From image descriptions to visual denotations: New similarity metrics for semantic inference over event descriptions," *Transactions of the Association for Computational Linguistics*, pp. 67–78, 2014.
- [31] O. Vinyals, A. Toshev, S. Bengio, and D. Erhan, "Show and tell: A neural image caption generator," in *Proceedings of the IEEE Conference on Computer Vision and Pattern Recognition*. IEEE, 2015, pp. 3156–3164.
- [32] D. Tran, L. Bourdev, R. Fergus, L. Torresani, and M. Paluri, "Learning spatiotemporal features with 3d convolutional networks," in *Computer Vision (ICCV), 2015 IEEE International Conference on*. IEEE, 2015, pp. 4489–4497.
- [33] A. Karpathy, G. Toderici, S. Shetty, T. Leung, R. Sukthankar, and L. Fei-Fei, "Large-scale video classification with convolutional neural networks," in *Proceedings of the IEEE Conference on Computer Vision and Pattern Recognition*, 2014.



Aditya Chattopadhyay is currently a Research Assistant in the Department of Computer Science and Engineering, Indian Institute of Technology Hyderabad, India. He received the Bachelor of Technology degree in Computer Science and Master of Science by Research degree in Computational Natural Sciences from the International Institute of Information Technology, Hyderabad in 2016 and 2018 respectively. His research interests include explainable Artificial Intelligence (X-AI), statistical modeling and theoretical aspects of machine learning with a special focus on optimization. He was awarded the Gold Medal for Academic Excellence in the master's program in computational natural sciences in 2018.



Anirban Sarkar is currently a doctoral student in the Department of Computer Science and Engineering, Indian Institute of Technology Hyderabad, India. He received the Master of Technology degree in computer science from National Institute of Technology, Rourkela, India, in 2016. He worked in IBM India as systems engineer for two and half years before joining the Masters program. His research interests include machine learning for computer vision, explainability of machine learning models and applications of causality in machine learning with a specific focus on deep learning.



Prantik Howlader is currently a software engineer and machine learning researcher in the Cisco Security Business Group, India. He received the M.Tech degree in computer science from National Institute of Technology, Calicut, India, in 2016. His research interests include Security, explainable AI and machine learning.



Vineeth N Balasubramanian is an Associate Professor in the Department of Computer Science and Engineering at the Indian Institute of Technology, Hyderabad, India. His research interests include deep learning, machine learning, computer vision, non-convex optimization and real-world applications in these areas. He has around 60 research publications in premier peer-reviewed venues including CVPR, ICCV, KDD, ICDM, IEEE TPAMI and ACM MM, as well as an edited book on a recent development in machine learning called Conformal Prediction. His PhD dissertation at Arizona State University on the Conformal Predictions framework was nominated for the Outstanding PhD Dissertation at the Department of Computer Science. He is an active reviewer/contributor at many conferences such as ICCV, IJCAI, ACM MM and ACCV, as well as journals including IEEE TNNLS, Machine Learning and Pattern Recognition.

APPENDIX A

SUPPLEMENTARY MATERIALS

We herein present further experimental results to confirm the effectiveness of Grad-CAM++. In the main text, we carried out all experiments with the VGG-16 architecture. To show that our results are not biased by the choice of CNN architecture, we carry out extensive experiments using both AlexNet [19] and ResNet-50 [20] architectures. For all experiments, the activation maps A^k considered were the last convolutional feature maps of the network (as in the main text for VGG-16). This appendix is organized as follows:

- We first present results from objective evaluation of performance of the two explanation algorithms, viz Grad-CAM and Grad-CAM++ for both AlexNet and ResNet-50 architectures, similar to the one carried out in Section 4.1 of the main text.
- This is followed by visual examples showing proof-of-concept of Grad-CAM++ in solving the problems of poor localization and multiple occurrences of the same class in an image.
- Lastly, we present visualizations of 3D action recognition decisions of a CNN, using both Grad-CAM and Grad-CAM++ (results from Section 6.2).

A.1 Objective Evaluation of Object Recognition Performance

The experimental setup in this section is the same as described in Section 4.1 of the main text, with the only difference being the CNN architecture used. Tables 7 and 8 report results for experiments carried out using AlexNet while Tables 9 and 10 outline the empirical results for the ResNet-50 architecture. These results follow a similar trend as seen in Tables 1 and 2 in the main text. Through extensive empirical experiments (Section 6.2 and Section 4.1 in the main text), we show that Grad-CAM++ visualizations are more faithful to the underlying deep model than Grad-CAM.

We note in passing that there seems to be a correlation between the "Average drop %" metric (for both Grad-CAM and Grad-CAM++) and the generalization prowess of the deep network it tries to explain. Resnet-50 has the lowest top-1 and top-5 classification error on the ImageNet dataset, followed by VGG-16 and subsequently AlexNet [17], [20]. For ImageNet the "Average drop %" metric for ResNet-50 (28 – 31%), VGG-16 (36 – 47%) and AlexNet (62 – 83%) follows the same trend. This correlation also exists for the Pascal VOC dataset. *This observation can potentially be exploited to prevent over-fitting and help deep networks learn more general features from data.*

A.2 More Visual Results

More visual results for Grad-CAM++ are shown in Fig. 8 corresponding to AlexNet and Fig. 9 corresponding to the ResNet-50 architecture.

A.3 Results for 3D Action Recognition

For action recognition using 3D CNN, we selected windows of 16 frames from each video to train the model. Sample qualitative results are presented as MPEG files along with

Method	Grad-CAM++	Grad-CAM
- Average drop% (Lower is better)	62.75	82.86
- % incr. in confidence (Higher is better)	8.24	3.16
- Win% (Higher is better)	86.56	13.44

TABLE 7

Results for objective evaluation of the explanations generated by both Grad-CAM++ and Grad-CAM on the ImageNet (ILSVRC2012) validation set ("incr" denotes increase). The explanations were generated for decisions taken by the **AlexNet** architecture.

Method	Grad-CAM++	Grad-CAM
- Average drop% (Lower is better)	29.16	45.82
- % incr. in confidence (Higher is better)	19.76	14.38
- Win% (Higher is better)	72.79	27.21

TABLE 8

Results for objective evaluation of the explanations generated by both Grad-CAM++ and Grad-CAM on the Pascal VOC 2007 validation set (2510 images) ("incr" denotes increase). The explanations were generated for decisions taken by the **AlexNet** architecture.

the Supplementary Material. The file names indicate the predicted action by the CNN model. For example, tennis.mpg, tennis_gcam.mpg and tennis_gcam++.mpg refer to the original 16 frame video, the explanation maps generated using Grad-CAM and explanation maps generated using Grad-CAM++ respectively. A few examples have also been shown in Figure 10, where the 16 frames video is truncated to 6 frames for clearer presentation. In both scenarios, the explanations generated by Grad-CAM++ are more semantically relevant. (The enclosed MPEG files provide a better visualization of our claim.)

Method	Grad-CAM++	Grad-CAM
- Average drop% (Lower is better)	28.90	30.36
- % incr. in confidence (Higher is better)	22.16	22.11
- Win% (Higher is better)	60.51	39.49

TABLE 9

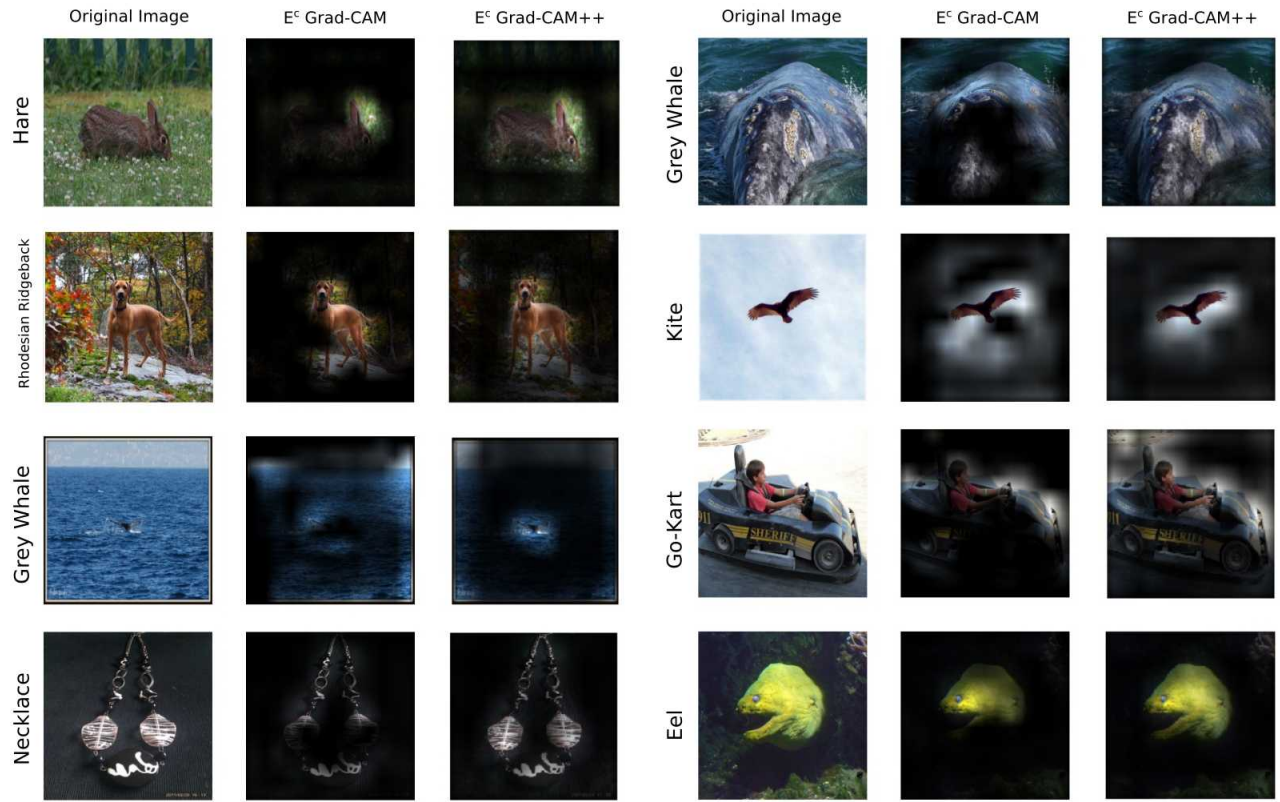
Results for objective evaluation of the explanations generated by both Grad-CAM++ and Grad-CAM on the ImageNet (ILSVRC2012) validation set ("incr" denotes increase). The explanations were generated for decisions taken by the **ResNet-50** architecture.

Method	Grad-CAM++	Grad-CAM
- Average drop% (Lower is better)	16.19	20.86
- % incr. in confidence (Higher is better)	19.52	21.99
- Win% (Higher is better)	58.61	41.39

TABLE 10

Results for objective evaluation of the explanations generated by both Grad-CAM++ and Grad-CAM on the Pascal VOC 2007 validation set (2510 images) ("incr" denotes increase). The explanations were generated for decisions taken by the **ResNet-50** architecture.

A



B

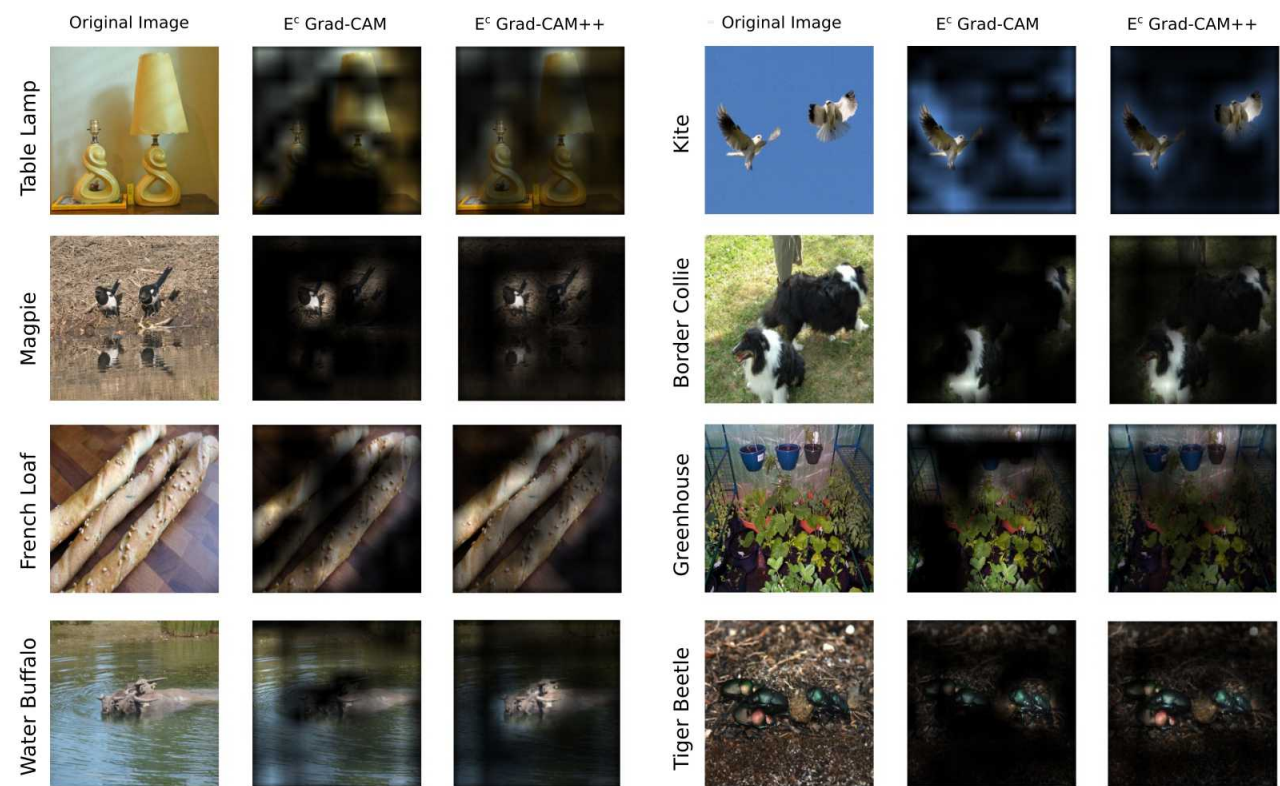
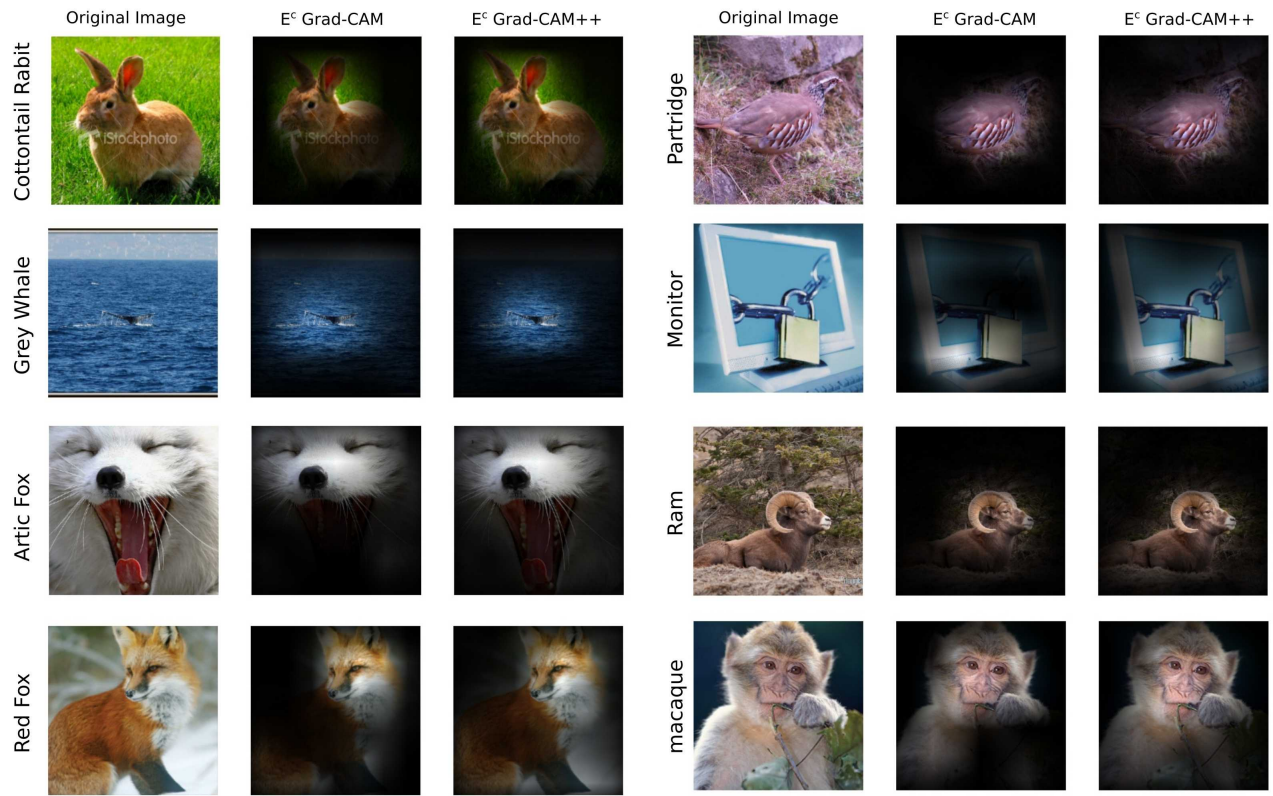


Fig. 8. Example explanation maps E^c (see Eq. 23 in main text) for images generated by Grad-CAM and Grad-CAM++. These explanations are for decisions made by the **AlexNet** architecture. Panel A shows images where Grad-CAM++ solves the problem of poor class localization. Panel B depicts images where Grad-CAM++ is effective for explaining multiple occurrences of the same class in an image. For each set of three images the class label predicted by the network is written horizontally on the leftmost edge.

A



B

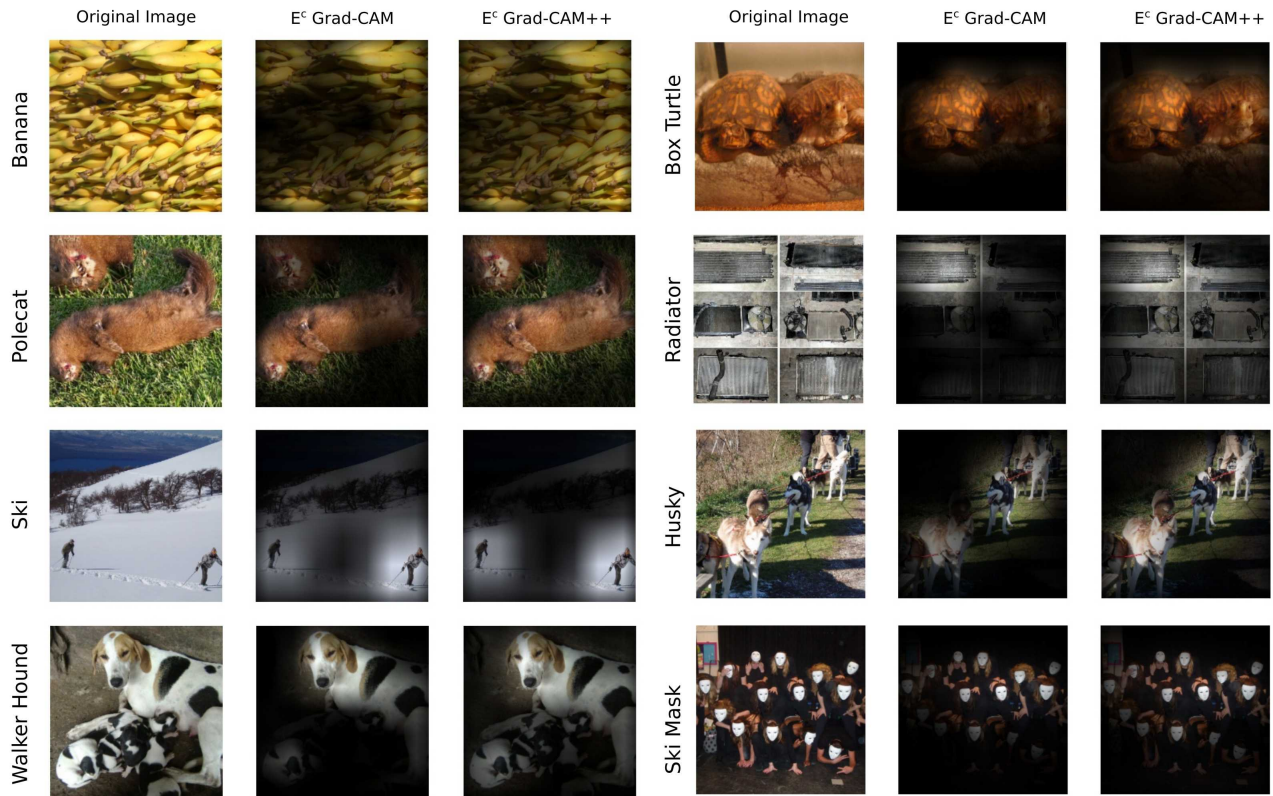


Fig. 9. Example explanation maps E^c (see Eq. 23 in main text) for images generated by Grad-CAM and Grad-CAM++. These explanations are for decisions made by the **ResNet-50** architecture. Panel A shows images where Grad-CAM++ solves the problem of poor class localization. Panel B depicts images where Grad-CAM++ is effective for explaining multiple occurrences of the same class in an image. For each set of three images the class label predicted by the network is written horizontally on the leftmost edge.



Fig. 10. Example explanation maps E^c (see Eq. 23 in main text) for video frames generated by Grad-CAM and Grad-CAM++ for a particular predicted action. The first set of video frames correspond to the predicted action "indoor soccer" and the next set of video frames correspond to "one day international". In the "indoor soccer" example, the E^c 's generated by Grad-CAM++ highlight the entire football ground with special emphasis on the two players, while Grad-CAM only highlights parts of the player's body. In the second set of video frames, the Grad-CAM++ explanations highlight the scoreboard with some importance to the players and pitch. The Grad-CAM interpretation of the model's decision on the other hand is bland.